Proposal of novel chatter stability indices of spindle speed variation based on its chatter growth characteristics

Soohyun Nam[a,*], Takehiro Hayasaka[a], Hongjin Jung[a], and Eiji Shamoto[a]

[a] Department of Aerospace Engineering, Graduate School of Engineering, Nagoya University, Furo-cho, Chikusa-ku, Nagoya, 464-8603, Japan

Abstract

Chatter is one of the most critical problems that causes poor surface quality and restriction of machining efficiency. Spindle speed variation (SSV) is a well-known technique for suppression of regenerative chatter. However, in the authors' understanding, the chatter suppression effect diminishes when the spindle speed difference between the present and previous cutting moments is small. Furthermore, the stability changes largely according to the spindle speed variation profile which changes with the set condition of SSV parameters, e.g., nominal spindle speed, variation period and variation amplitude. Therefore, SSV parameters should be adequately set to avoid this limitation and to exert its effect throughout the entire duration of cutting. However, there is no clear methodology to determine the optimal condition. This paper presents the characteristics of chatter growth during SSV focusing on the change of chatter frequency, which lead to novel indices to evaluate the chatter stability when cutting with SSV. To verify the validity of the indices, time-domain simulations and the cutting experiments with triangular spindle speed variation (TSSV) are carried out. The influence of SSV parameters on the chatter stability is investigated from the simulation and experimental results. The limitations of widely utilized SSV profiles are discussed.

Keywords : Regenerative chatter; Spindle speed variation; Acceleration rate;.

1 Introduction

During the machining processes, the instability from the interaction between the metal cutting process and response of machine tool structure results in chatter. The chatter causes poor surface finish, excessive tool wear, and damage of the machine tool. The chatter usually occurs in conditions above a certain limit of cutting width or structural flexibility. In general, it can be avoided by lowering the cutting conditions, e.g., cutting width, but it leads to low machining efficiency. Extensive studies have been performed in order to clarify the mechanism of chatter, and it has been revealed that the self-excited vibration caused by the regenerative effect, i.e., regenerative chatter, is the most dominant machine tool chatter phenomenon [1]. The regenerative effect is caused by the previous vibration which is left on the workpiece as a wavy surface. The regenerative chatter grows up with a certain phase shift between the present and previous vibrations which causes dynamic chip load.

To suppress the regenerative chatter and to increase the stability and machining efficiency, various studies have been carried out, e.g., the selection of stable cutting conditions such as spindle speed and depth of cut [2], the optimization of tool path/posture [3], the usage of specially designed milling tools with variable pitch/helix angles [4, 5], and the optimization and the design methodology of those special tools [6, 7]. As another effective method for the suppression of the regenerative chatter without sacrificing the machining efficiency, the spindle speed variation (SSV) has been studied, where the speed is varied around the nominal spindle speed. Takemura et al. [8] analyzed its stability in the turning process by means of energy balance and validated it through experiments. After that, numerous types of analytical methods have been proposed such as the angle domain method [9], the semidiscretization method [10], the method using the SSV frequency harmonics of chatter vibration [11], etc.

Several profiles have been proposed to vary the spindle speed such as sinusoidal, triangular, rectangular, and random profiles. It is well known that the sinusoidal spindle speed variation (SSSV) can be easily applied by the spindle speed control system with low load compared to the other profiles, hence it is the most popular technique [12]. The triangular spindle speed variation (TSSV) has also been developed

to suppress the regenerative chatter (e.g., OKUMA Corp. Machining Navi L-*g*), and it is usefully utilized in production sites.

Meanwhile, since the stability of SSV varies greatly depending on the SSV parameters, i.e., variation amplitude, variation period, and nominal spindle speed, it is quite a complicated problem to determine the parameters properly [13, 14]. For example, in the case of the same variation amplitude, SSV yields higher stability at lower nominal speed [13, 14]. Furthermore, the temporal growth of chatter occurs even if SSV is applied [13-15]. For this problem, despite the fact that SSV is an effective technique, the industrial application has been limited because there is no simple and logical methodology to determine the parameters properly for the suppression of chatter and the improvement of the machining efficiency. Therefore, there is a need for a general index to evaluate the stability of SSV.

In this research, characteristics of the chatter growth in SSV are clarified and the chatter stability indices are newly proposed based on them. Time-domain simulations and cutting experiments are carried out, and the validity of the proposed indices and the effect of the SSV parameters on the stability are discussed.

The dynamic cutting model and the basic principle of the chatter stability prediction with constant spindle speed (CSS) is described in Section 2.1. In Section 2.2, the characteristics of the chatter growth in SSV are explained. The novel chatter stability indices for SSV and the analytical investigations with a time-domain simulation model are presented in Section 3. In Section 4, the experimental results and their discussions are described. Conclusions of the paper follow in Section 5.

2 Characteristics of chatter growth in SSV

2.1 Dynamic model of orthogonal cutting process

A dynamic model of a pipe-end plunging process, which can be considered as a semi-orthogonal cutting process, is shown in Fig. 1. It is assumed that the tool shank is flexible in the cutting (y) and feed (z) directions. In this process, the vibration in the z direction causes the fluctuation of the principal (y) and thrust (z) cutting forces.

Not only the present vibration but also the previous vibration left on the cut surface affect the present cutting; the latter one is called the regenerative effect. Those vibrations cause the uncut chip thickness fluctuation, and it results in the dynamic cutting force. Since the cutting force is proportional to the instantaneous uncut chip thickness $h(t)$ [m], which can be expressed as Eq. (1), the dynamic cutting forces in the principal direction f_y [N] and the thrust direction f_z [N] can be formulated as Eq. (2). Note that the formulation is in the Laplace domain after Eq. (1).

$$h(t) = h_0 + \mu z(t-\tau) - z(t) \tag{1}$$

$$\begin{Bmatrix} f_y \\ f_z \end{Bmatrix} = a(e^{-s\tau} - 1) \begin{bmatrix} 0 & K_y \\ 0 & K_z \end{bmatrix} \begin{Bmatrix} y \\ z \end{Bmatrix} \tag{2}$$

Here, h_0 [m] is the static depth of cut, i.e., feed rate of the cutting tool, μ is the overlapping factor ($\mu = 1$ in pipe-end plunging), τ [s] is the spindle period, a [m] is the cutting width, K_y [Pa] and K_z [Pa] are the specific cutting forces in the principal and thrust directions, respectively, and y [m] and z [m] are the dynamic displacements in the principal and thrust directions, respectively. Note that the static depth of cut h_0 has no effect on the dynamic cutting forces, hence it does not exist in Eq. (2).

The dynamic cutting forces excite the tool shank, and they cause the vibration displacements through the dynamic compliances as follows.

$$\begin{Bmatrix} y \\ z \end{Bmatrix} = \begin{bmatrix} G_{yy} & G_{yz} \\ G_{zy} & G_{zz} \end{bmatrix} \begin{Bmatrix} f_y \\ f_z \end{Bmatrix} \tag{3}$$

Here, G_{yy} [m/N] and G_{zz} [m/N] are the direct dynamic compliances in the principal and thrust directions, respectively, and G_{yz}[m/N] and G_{zy} [m/N] are the cross dynamic compliances between the principal and thrust directions.

Since the vibration in the principal (y) direction does not cause the dynamic uncut chip thickness, the closed-loop system with the cutting process and the equivalent dynamic compliance [16] can be represented as the block diagram shown in Fig. 2. Combining Eqs. (2) and (3), the following equation can be derived under critical stability at the angular chatter frequency ω_c [rad/s].

$$z(i\omega_c) = a_{lim}K_z\left(e^{-i\omega_c\tau} - 1\right)G_z(i\omega_c)z(i\omega_c). \quad (4)$$

Here, G_z [m/N] is the equivalent dynamic compliance, i.e., $G_z = G_{zz} + K_y/K_z \times G_{zy}$, where K_y/K_z is the cutting force ratio. The stability limit analysis is performed by solving Eq. (4), i.e., the critical cutting width or stability limit a_{lim} [m] and the corresponding spindle period τ [s] are calculated. As a result, a_{lim} is given as follows [17].

$$a_{lim} = -\frac{1}{2K_z\Lambda_{re}} \quad (5)$$

Here, Λ_{re} is the real part of the equivalent dynamic compliance.

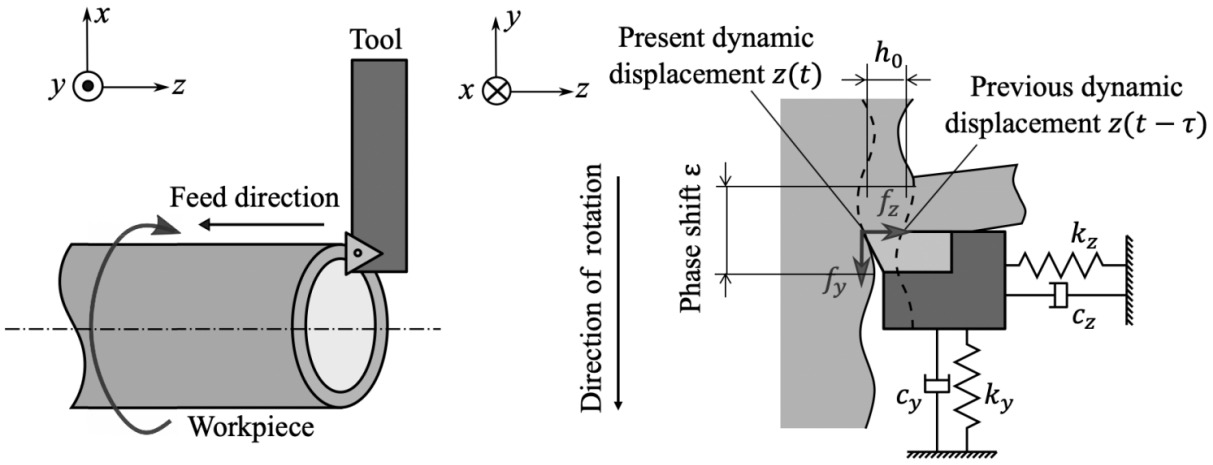

Fig. 1. Dynamic model of pipe-end plunging process.

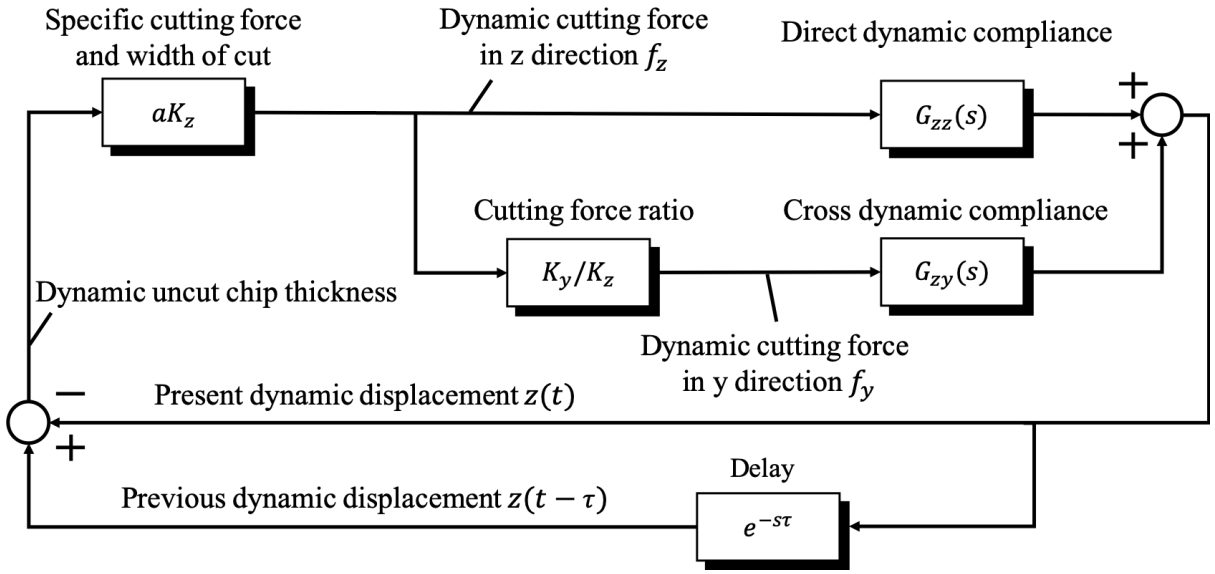

Fig. 2. Block diagram of pipe-end plunging process with regenerative effect.

2.2 Chatter growth / suppression in SSV

Due to the nature of the cutting process, the chatter is transferred to the workpiece as a wavy surface. After one revolution, the difference between the wavy surface and the present vibratory locus of the cutting edge causes the cutting force fluctuation. The regenerative chatter leaves a number of waves on the cut surface per unit angle, i.e., spatial chatter frequency f_{sc} [1/rad]. It can be expressed as Eq. (6), and its schematic illustration is shown in Fig. 3. Note that to visually imagine the concept, the figure is drawn as a plunge-turning process where the vibration waves can be seen easily, but it is the same in other cutting processes.

$$f_{sc} = \frac{60 f_c(t)}{2\pi n(t)} = \frac{30 f_c(t)}{\pi n(t)} \tag{6}$$

Here, $n(t)$ [min^{-1}] and $f_c(t)$ [Hz] are the spindle speed and the chatter frequency on the time t, respectively. From Eq. (6), the chatter frequency $f_c(t)$ can be described as follows.

$$f_c(t) = \frac{2\pi n(t) f_{sc}}{60} \tag{7}$$

In the case of CSS, $f_c(t)$ is constant since $n(t)$ is constant during the machining. Even when SSV is applied, the regenerative chatter can grow with a considerably flexible structure. It is found in this study that the regenerative chatter generally grows at a constant spatial frequency in SSV (the first chatter growth characteristic), i.e., the time chatter frequency changes with varying spindle speed, unlike the assumption of constant time chatter frequency in previous studies [8-14, 18]. The varied time chatter frequency can be expressed as follows.

$$f_c(t) = \frac{n(t)}{n\big(t-\tau(t)\big)} f_c(t-\tau(t)) \tag{8}$$

Here, $\tau(t)$ [s] is the spindle period which varies depending on the spindle speed profile, $n\big(t-\tau(t)\big)$ and $f_c(t-\tau(t))$ are the spindle speed and the chatter frequency at one revolution before, respectively.

As a result, the time chatter frequency changes proportionally to the rate of spindle speeds in two consecutive revolutions at the same angular position, i.e., acceleration rate r_a [%], and it can be expressed as follows [15].

$$r_a(t) = \left(\frac{n(t)}{n\big(t-\tau(t)\big)} - 1\right) \times 100 \tag{9}$$

Here, since the chatter tends to occur near the resonance, the changes of the chatter frequency in SSV causes a large change of the amplitude of the present vibration $z(t)$ [m] due to the change of the magnitude of the dynamic compliance of the vibratory structure $G_z\big(i\omega_c(t)\big)$ [m/N], and it can be expressed as follows.

$$G_z\big(i\omega_c(t)\big) = G_z\left(i\left(\left(1+\frac{r_a(t)}{100}\right)\times \omega_c\big(t-\tau(t)\big)\right)\right) \tag{10}$$

$$z(t) = G_z\big(i\omega_c(t)\big) f_z(t) = G_z\left(i\left(\left(1+\frac{r_a(t)}{100}\right)\times \omega_c\big(t-\tau(t)\big)\right)\right) f_z(t) \tag{11}$$

Note that the larger r_a, the larger the change of chatter frequency and the change of magnitude of dynamic compliance, and the cutting becomes more stable [15]. Therefore, it can be estimated that the chatter is likely to grow if there is a period where r_a is small in SSV (the second chatter growth characteristic).

Next, in case of considering plural revolutions, e.g., more than two revolutions, the chatter frequency after m-revolutions at a certain angular position f_m [Hz] can be expressed as Eq. (12).

$$f_m = \frac{n_m}{n_{m-1}}\frac{n_{m-1}}{n_{m-2}}\cdots\frac{n_1}{n_0}\times f_0 = \frac{n_m}{n_0}\times f_0 \tag{12}$$

Here, n_0 [min^{-1}] and f_0 [Hz] are the initial spindle speed and the initial chatter frequency, respectively. As the ratio of n_m to n_0 increases, the change of chatter frequency becomes larger and it results in larger

dynamic compliance reduction, and the system becomes more stable. However, it should be noted that chatter can grow when the reduction of the dynamic compliance in each revolution is insufficient to suppress chatter. Also, the peakiness of the dynamic compliance, which increases with a decrease of the damping coefficient, as well as the cross dynamic compliance, also affect the change rate of the magnitude of the dynamic compliance, hence it can affect the degree of the chatter suppression.

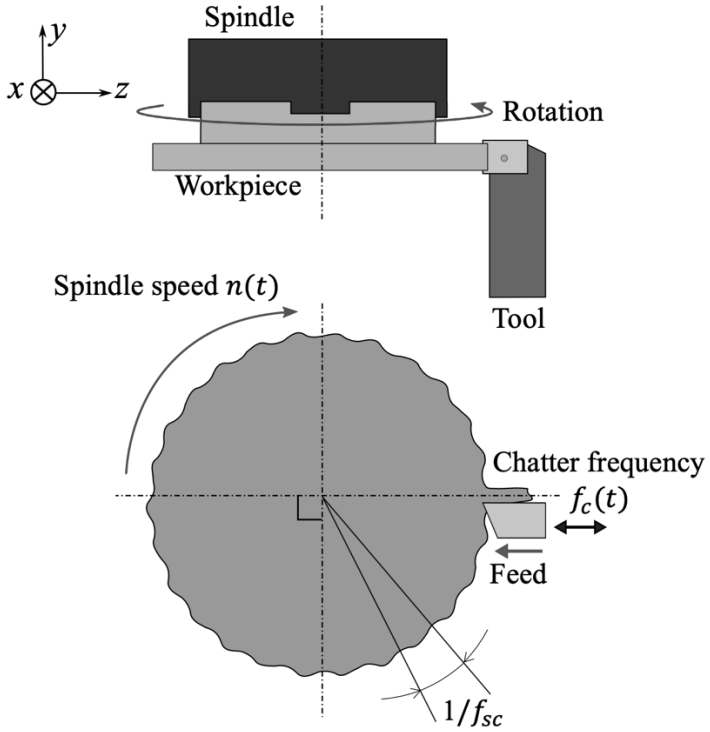

Fig. 3. Schematic illustration of plunge-turning process with regenerative chatter.

3 Analytical investigation of chatter stability in SSV

3.1 Time-domain simulation model

To verify the validity of the revealed chatter growth characteristics in SSV and to investigate the relation between the acceleration rate r_a and the stability in TSSV and SSSV, time-domain simulations are carried out. A single degree of freedom (SDOF) vibratory system with orthogonal cutting shown in Fig. 1 is assumed. Here, the cutting tool is flexible and the regeneration occurs in the thrust direction (z). The uncut chip thickness $h(t)$ [mm] and the cutting force in the thrust direction $f_z(t)$ [N] fluctuates when chatter occurs, and each of them can be expressed as follows.

$$h(t) = h_0 + \mu z(t - \tau(t)) - z(t) \tag{13}$$

$$f_z(t) = K_z a h(t) \tag{14}$$

The response of the cutting tool to the cutting force in the SDOF system can be described as follows.

$$m\ddot{z}(t) + c\dot{z}(t) + kz(t) = K_z a(h_0 + \mu z(t - \tau(t)) - z(t)) \tag{15}$$

Here, m [kg] is the modal mass, c [N/(m·s)] is the modal damping coefficient, k [N/m] is the modal stiffness, and μ =1 in pipe-end plunging. Note that in the case of cutting with SSV, the spindle period $\tau(t)$ varies with time due to the time-varying spindle speed $n(t)$ [min^{-1}], and it can be searched to satisfy the following equation.

$$\int_{t-\tau(t)}^{t} \frac{n(t)}{60} dt = 1 \tag{16}$$

In the time-domain simulation, $z(t)$ is calculated by solving Eq. (15) directly, and the solution is approximated by the 4th order Runge-Kutta method. Here, the accumulated rotation angle $\theta(t)$ [rad], which can be expressed as Eq. (17), $z(t)$ and $n(t)$ are memorized at each calculation step, i.e., resolution of time-domain simulation, and they are utilized when searching the previous displacement $z(\theta(t)-2\pi)$ and the previous spindle speed $n(\theta(t)-2\pi)$.

$$\theta(t) = 2\pi \int_0^t \frac{n(t)}{60} dt \tag{17}$$

The tool jumping out of the workpiece, i.e., $h(t) = 0$, due to the vibration is considered in the simulation. At the beginning of simulation, the cutting starts with gradually increasing static depth of cut.

3.2 Formulation of SSV profiles and introduction of stability indices

Since the triangular and the sinusoidal spindle speed variation, i.e., TSSV and SSSV, profiles are considered in most literatures [9-14, 18], they are investigated in the current study. The schematics for the explanation of the spindle speed and acceleration rate profiles in TSSV and SSSV are shown in Fig. 4 (a) and Fig. 4 (b), respectively. Here, n_0 [min^{-1}] is the nominal spindle speed, T [s] is the variation period, and n_A [min^{-1}] is the variation amplitude, respectively. The variation function of TSSV $n_{tri}(t)$ [min^{-1}] can be described as follows.

$$n_{tri}(t) = \begin{cases} n_0 + n_A - \dfrac{4n_A}{T}\mathrm{mod}(t,T) & \text{if} \quad 0 \le \mathrm{mod}(t,T) < T/2 \\ n_0 - 3n_A + \dfrac{4n_A}{T}\mathrm{mod}(t,T) & \text{if} \quad T/2 \le \mathrm{mod}(t,T) < T \end{cases} \tag{18}$$

Here, $\mathrm{mod}(t,T)$ denotes the modulo function.

The variation function of SSSV $n_{sin}(t)$ [min^{-1}] can be described as follows.

$$n_{sin}(t) = n_0 + n_A \sin\left(\frac{2\pi}{T}t + \frac{\pi}{2}\right) \tag{19}$$

As observed in Figure 4, the acceleration rate r_a always fluctuates with the speed variation. The r_a has a positive value in the acceleration section and has a negative value in the deceleration section. At the sections where the acceleration direction is switched, i.e., switching from acceleration to deceleration or from deceleration to acceleration, the speed difference in two consecutive revolutions is nearly zero, and the value of r_a is close to zero. Since the length of these sections should be one revolution, i.e., 2π rad, the time lengths t_1, t_2 should satisfy the following equations.

$$\int_{\frac{T}{2}}^{\frac{T}{2}+t_1} \frac{n(t)}{60} dt = 1 \tag{20}$$

$$\int_{T}^{T+t_2} \frac{n(t)}{60} dt = 1 \tag{21}$$

Since r_a fluctuates in SSV, the average of absolute acceleration rate in one period of SSV $\overline{|r_a|}$ [%] is utilized as the stability index for evaluating the stability in SSV, and it can be expressed as follows.

$$\overline{|r_a|} = \frac{1}{T}\int_0^T |r_a(t)|\, dt = \frac{100}{T}\int_0^T \left|\left(\frac{n(t)}{n\big(t-\tau(t)\big)} - 1\right)\right| dt \tag{22}$$

Meanwhile, when considering the plural revolutions in a unidirectional acceleration section, the more revolutions show the larger change of the dynamic compliance since the chatter frequency also changes largely in one way, i.e., increase or decrease, as shown in Eq. (12). From this observation, the number of revolutions in a unidirectional acceleration section N is utilized as the second stability index for evaluating the stability in SSV, and it can be calculated from SSV parameters as follows.

$$N = \frac{n_0}{60}\frac{T}{2} = \frac{n_0 T}{120} \tag{23}$$

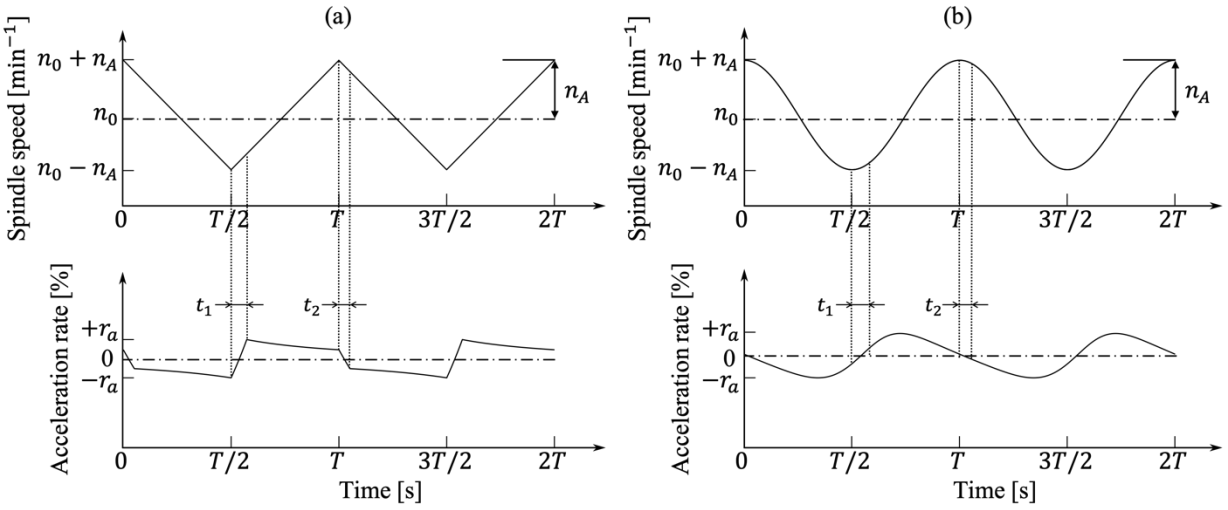

Fig. 4. Profiles of spindle speed and acceleration rate in (a) TSSV and (b) SSSV.

3.3 Simulation conditions and profile examples

The utilized parameters in the time-domain simulation are shown in Table 1. To investigate the validity of the proposed stability indices, i.e., $\overline{|r_a|}$ and N, the SSV parameters are determined so that TSSV and SSSV have the same stability indices. Note that the variation amplitude ratio RVA, which is defined as the ratio of the speed variation amplitude to the nominal spindle speed n_A/n_0, should be set lower than 1 so that the spindle speed is always higher than 0. Thus, the range of RVA is set from 0.05 to 0.80. The cutting width is gradually increased with increments of 0.1 mm, and the stability limit is found. In this simulation, the growing vibration in each period of SSV is considered as chatter.

Table 1. Parameters used in time-domain simulation.

Workpiece properties		
Diameter D	[mm]	70
Specific cutting force in principal direction K_y	[MPa]	1284
Specific cutting force in thrust direction K_z	[MPa]	711
Modal parameters		
Mass m	[kg]	0.2266
Damping coefficient c	[N/(m·s)]	44.19
Stiffness k	[N/m]	1.118×10^7
SSV parameters		
Nominal spindle speed n_0	[min^{-1}]	600 - 7200
Variation period T	[s]	0.5, 1.0, 2,0
Variation amplitude ratio RVA		0.05 - 0.80
Cutting conditions		
Feed rate (static depth of cut) h_0	[mm/rev]	0.05
Increment of cutting width	[mm]	0.1

Figures 5(a) and 5(b) show examples of unstable results in TSSV and SSSV, respectively. In both profiles, the growth of chatter is observed in the transitions from the acceleration to the deceleration. On the other hand, the chatter does not grow in the transitions from the deceleration to acceleration. This can be explained as follows: the acceleration rate in the lower speed is larger than that in the higher speed, and hence the chatter suppression effect is greater in the lower speed. As a result, there is a chatter growth

characteristic that it grows in the transitions from the acceleration to the deceleration where the acceleration rate $|r_a|$ is small.

The change of the chatter frequency can be observed in the short-time Fourier transform result of vibration displacement in each graph, i.e., as the spindle speed decreases, the chatter frequency decreases in a similar way. In order to clarify the chatter growth characteristics quantitatively, the spatial frequency f_{sc} during chatter is investigated. Comparisons of the points A, B and C, D in Figure 5 are carried out. The spindle speeds at points of A, B and C, D are 1120 min^{-1}, 1070 min^{-1} and 1155 min^{-1}, 1110 min^{-1}, respectively. The chatter frequencies at points of A, B and C, D are 1195 Hz, 1145 Hz and 1170 Hz, 1115 Hz, respectively. Finally, the spatial frequencies at points A, B and C, D are calculated by utilizing the Eq. (6), and their values are 10.19, 10.22 and 9.67, 9.59, respectively. From the results, it can be confirmed that the spatial frequencies at the points A, B and C, D are nearly the same. Therefore, it can be concluded that the chatter frequency generally changes in proportion to the spindle speed, i.e., the chatter grows up at a constant spatial frequency in SSV.

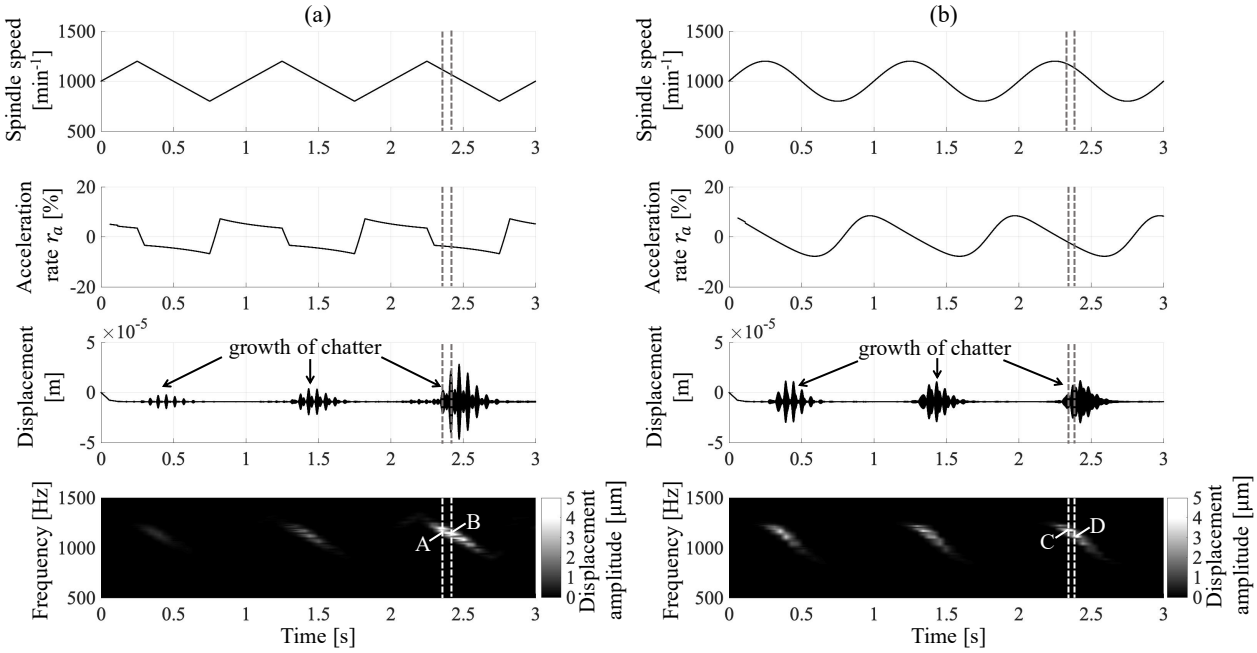

Fig. 5. Profile examples of spindle speed and acceleration rate, and corresponding vibration displacement and its short-time Fourier transform result of unstable condition at cutting width=2.9 mm, n_0=1000 min^{-1}, T=1.0 sec, and RVA=0.2 in (a) TSSV and (b) SSSV.

3.4 Simulation results and discussions

The relations between the stability limit and the proposed stability indices, i.e., $\overline{|r_a|}$ and N, in TSSV and SSSV are investigated by utilizing the time-domain simulation model. Figure 6 shows the simulation results under various conditions: (a) TSSV, T=0.5 sec (b) SSSV, T=0.5 sec, (c) TSSV, T=1.0 sec, (d) SSSV, T=1.0 sec, (e) TSSV, T=2.0 sec and (f) SSSV, T=2.0 sec. Since each graph represents the results obtained at a constant T, n_0 takes the proportional value with N from Eq. (23). The dotted lines indicate the contours where RVA is 0.2, 0.4, 0.6, and 0.8, respectively. Note that even if T and RVA are equal, the value of $\overline{|r_a|}$ decreases with an increase of n_0 or N. Finally, the magnitude of the stability limit is represented by gray scale. Figures 7(a) and 7(b) show the profile examples of spindle speed and acceleration rate which correspond to A to F marked on Figs. 6(c) and 6(d), respectively. The solid (A/D), dashed (B/E), and dotted (C/F) lines represent the profiles under the conditions of T=1.0 sec, $\overline{|r_a|}$=10 %, and N=5, 15, 25, respectively, in TSSV/SSSV. The spindle speed profiles show that the nominal spindle speed increases and

RVA also increases with an increase of N. The former tendency can be confirmed in Eq. (23), and the latter one is needed to keep $\overline{|r_a|}$ constant. From Figs. 6 and 7, the following five remarks are found.

First, it can be confirmed from Fig. 6 that when N is equal, the stability limit increases with an increase of $\overline{|r_a|}$ regardless of T and the type of SSV. Hence, $\overline{|r_a|}$ is an effective index for evaluating the stability of SSV.

Second, when $\overline{|r_a|}$ is equal, the stability is the largest at a certain N, e.g., 20 in the case of $\overline{|r_a|} = 10$ in Fig. 6(a). The reasons for this can be considered as follows. With an increase of N, the chatter frequency changes largely as expressed in Eq. (12), and thus the stability increases because the dynamic compliance is greatly reduced. On the other hand, it can be observed from the profiles of r_a in Fig. 7 that with an increase of N the fluctuation amplitude of r_a becomes large. Consequently, $|r_a|$ becomes smaller and that section becomes longer near the transitions from acceleration to deceleration. Therefore, a sufficient compliance reduction cannot be obtained in that section, and hence stabilization cannot be achieved at excessively large N. From these reasons, an optimal value of N exists.

Third, in the case where the values of $\overline{|r_a|}$ and N are equal in the same type of SSV, the stability limits are almost identical among different T's (Figs. 6(a)-(c) or (d)-(f)). Therefore, the stability limit can be estimated in each type of SSV by utilizing the two proposed stability indices regardless of the combination of SSV parameters.

Fourth, comparing the results in TSSV and SSSV, it can be confirmed that the stability limit in SSSV is always smaller than TSSV when $\overline{|r_a|}$ and N are equal. The reason for this is considered as follows. The shape of r_a profile is different and $|r_a|$ becomes smaller in SSSV than in TSSV near the transition from acceleration to deceleration as shown in Fig. 7. This can be observed more clearly in Fig. 4. Because of this period of smaller $|r_a|$, the stability in SSSV is always smaller than TSSV. When lower RVA is desirable, e.g., tool wear may progress rapidly at high speeds for difficult-to-cut materials, SSSV (Figs. 6(d)-(f)) can have relatively higher $\overline{|r_a|}$ and N compared to TSSV (Figs. 6(a)-(c)) under equal RVA. However, the stability in TSSV is larger than that in SSSV under equal RVA even though $\overline{|r_a|}$ and N are lower. For example, stability limits under $RVA = 0.6$, $T = 2.0$ sec, and equal $\overline{|r_a|}$ or N (G-K/G'-K' shown in Figs. 6(c)/6(f)) are estimated in TSSV/SSSV by linear interpolation between neighboring stability limits. The estimated values are (3.56 mm, 3.90 mm, 4.29 mm, 4.49 mm, 4.80 mm)/(3.39 mm, 3.59 mm, 3.72 mm, 4.31 mm, 4.45 mm), and it is confirmed that the stability in TSSV is always higher than that in SSSV under equal RVA.

Fifth, when RVA and T are equal, all the graphs represent that the smaller the N, i.e., the smaller the n_0, the higher the stability because $\overline{|r_a|}$ increases as n_0 decreases under equal RVA. In other words, the chatter suppression effect of TSSV and SSSV decreases in high-speed region, and thus it is unfortunately difficult to realize remarkable improvement of machining efficiency.

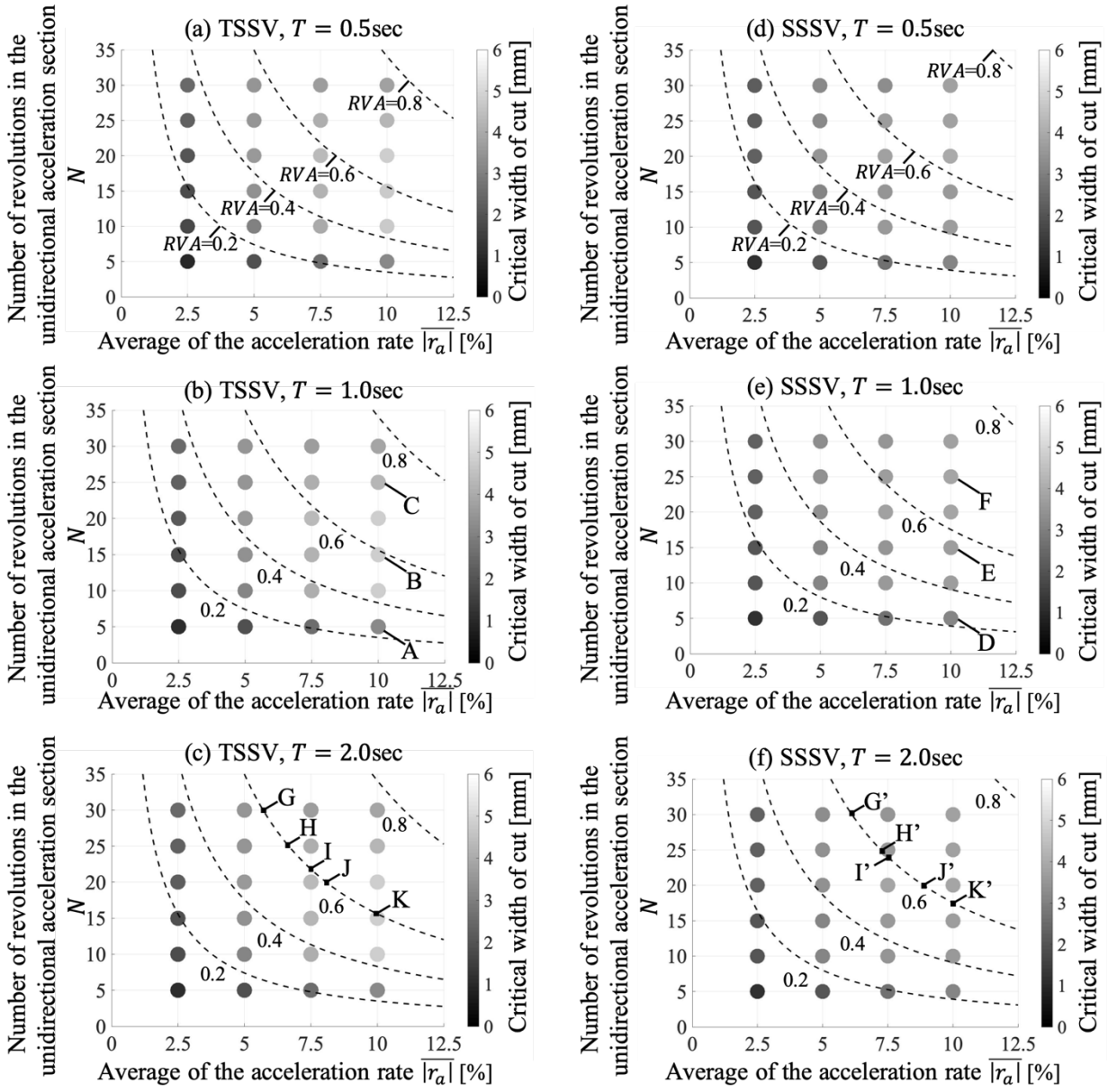

Fig. 6. Stability limits against the stability indices $\overline{|r_a|}$ and N under variable condition of T in TSSV and SSSV.

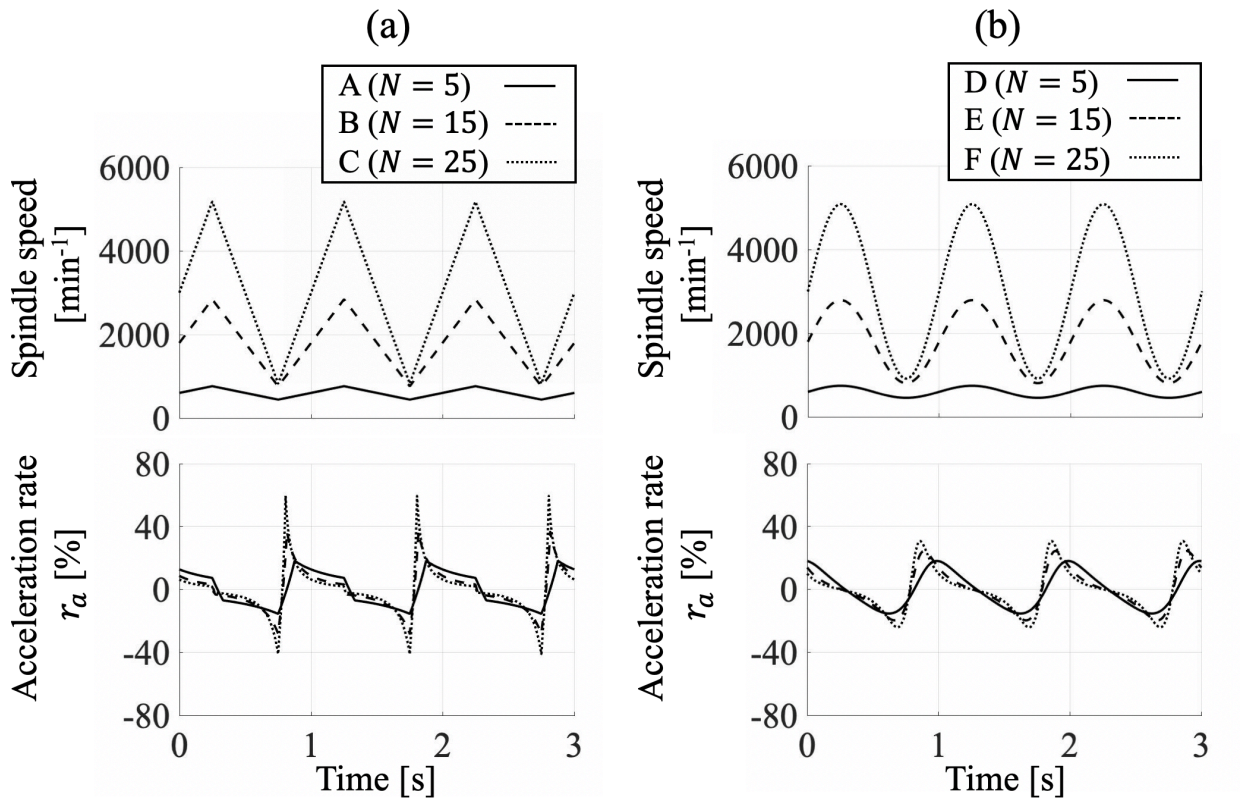

Fig. 7. Profile examples of spindle speed and acceleration rate under conditions of T=1.0 sec, $\overline{|r_a|}$=10 %, and N=5, 15, 25 in (a) TSSV and (b) SSSV.

4 Experimental verification

4.1 Experimental setup

A series of experiments are carried out to verify the validity of the revealed chatter growth characteristics in SSV and to confirm the effectiveness of the proposed stability indices, i.e., $\overline{|r_a|}$ and N. Figure 8 shows a photograph of the experimental setup for the pipe-end plunging. The experiments are conducted on a turning center (Okuma Corp., SPACETURN LB3000EX), and a pipe-shaped workpiece (brass, ISO CuZn35) is cut by a tool insert (Mitsubishi Material Corp., TCMW16T308 HTi10) mounted on a tool shank (steel, ISO C45) with a rectangular cross-section. The rake and clearance angles are 0 and 7 deg, respectively.

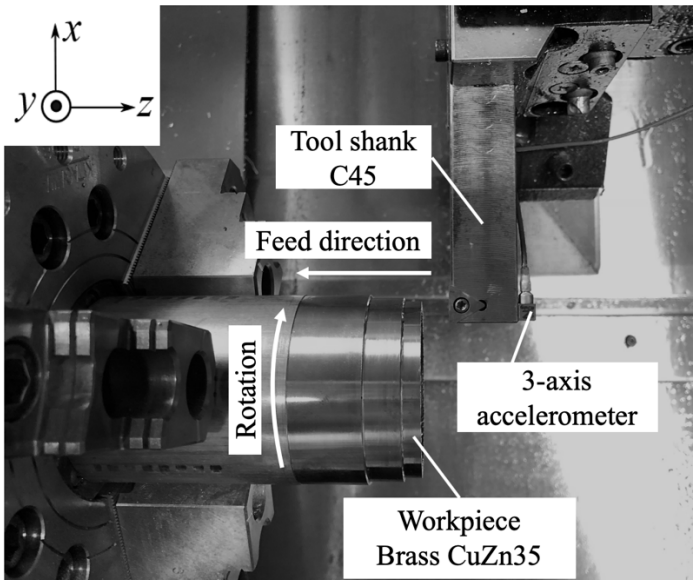

Fig. 8. Experimental setup for pipe-end plunging.

4.2 Measurement of dynamic compliance of tool

Measurement of the dynamic compliance of the tool is carried out with an impact hammer (PCB Electronics Inc., 084A14), an accelerometer (PCB Electronics Inc., 356A01), and a dummy tool insert with flat perpendicular faces for accurate force input. In order to increase the reliability of the measurement, the number of impacts for each direction is set to 10, and the average of the results is utilized in the time-domain simulations for comparison with the cutting experiments with TSSV.

The workpiece is rigid in the depth of cut (z) direction, and the projection of the tool shank is set as long as 90 mm, and thus the chatter occurs mainly due to the flexibility of the tool in the z direction. The measured dynamic compliances are shown in Fig. 9 where (a) shows the cross dynamic compliance and (b) shows the direct dynamic compliance. In order to use these compliances in the time-domain simulations, the modal parameters of the dynamic compliances, including the cross dynamic compliance whose phase changes complexly, are identified in the following manner. The equation of motion of the tool can be represented as follows.

$$[M]\begin{Bmatrix}\ddot{y}(t)\\ \ddot{z}(t)\end{Bmatrix}+[C]\begin{Bmatrix}\dot{y}(t)\\ \dot{z}(t)\end{Bmatrix}+[K]\begin{Bmatrix}y(t)\\ z(t)\end{Bmatrix}=\begin{Bmatrix}f_y(t)\\ f_z(t)\end{Bmatrix} \tag{24}$$

Here, $[M]$, $[C]$, and $[K]$ are the modal mass, damping coefficient, and stiffness matrices, and they are expressed as follows.

$$[M]=\begin{bmatrix}m_{yy} & m_{yz}\\ m_{zy} & m_{zz}\end{bmatrix},[C]=\begin{bmatrix}c_{yy} & c_{yz}\\ c_{zy} & c_{zz}\end{bmatrix},[K]=\begin{bmatrix}k_{yy} & k_{yz}\\ k_{zy} & k_{zz}\end{bmatrix} \tag{25}$$

Equation (24) can be represented in the s domain by taking the Laplace transform as follows.

$$([M]s^2+[C]s+[K])\begin{Bmatrix}y(s)\\ z(s)\end{Bmatrix}=\begin{Bmatrix}f_y(s)\\ f_z(s)\end{Bmatrix} \tag{26}$$

The dynamic displacements in the principal and thrust directions can be expressed as follows:

$$\begin{Bmatrix}y(s)\\ z(s)\end{Bmatrix}=([M]s^2+[C]s+[K])^{-1}\begin{Bmatrix}f_y(s)\\ f_z(s)\end{Bmatrix}\equiv\begin{bmatrix}G_{yy} & G_{yz}\\ G_{zy} & G_{zz}\end{bmatrix}\begin{Bmatrix}f_y(s)\\ f_z(s)\end{Bmatrix} \tag{27}$$

where the elements of the dynamic compliances can be expressed as follows.

$$G_{yy}=\frac{m_{zz}s^2+c_{zz}s+k_{zz}}{(m_{yy}s^2+c_{yy}s+k_{yy})(m_{zz}s^2+c_{zz}s+k_{zz})-(m_{yz}s^2+c_{yz}s+k_{yz})(m_{zy}s^2+c_{zy}s+k_{zy})} \tag{28}$$

$$G_{yz} = -\frac{m_{yz}s^2 + c_{yz}s + k_{yz}}{(m_{yy}s^2 + c_{yy}s + k_{yy})(m_{zz}s^2 + c_{zz}s + k_{zz}) - (m_{yz}s^2 + c_{yz}s + k_{yz})(m_{zy}s^2 + c_{zy}s + k_{zy})}$$

$$G_{zy} = -\frac{m_{zy}s^2 + c_{zy}s + k_{zy}}{(m_{yy}s^2 + c_{yy}s + k_{yy})(m_{zz}s^2 + c_{zz}s + k_{zz}) - (m_{yz}s^2 + c_{yz}s + k_{yz})(m_{zy}s^2 + c_{zy}s + k_{zy})}$$

$$G_{zz} = \frac{m_{yy}s^2 + c_{yy}s + k_{yy}}{(m_{yy}s^2 + c_{yy}s + k_{yy})(m_{zz}s^2 + c_{zz}s + k_{zz}) - (m_{yz}s^2 + c_{yz}s + k_{yz})(m_{zy}s^2 + c_{zy}s + k_{zy})}$$

Therefore, the equivalent dynamic compliance in the thrust direction, i.e., $G_z(s)$, can be calculated as follows.

$$G_z(s) = \{G_{zy}\ G_{zz}\}\begin{Bmatrix} K_y/K_z \\ 1 \end{Bmatrix} = K_y/K_z \times G_{zy} + G_{zz} \tag{29}$$

The modal parameters are numerically identified by utilizing the least squares method between the measured compliances and the fitted compliances which use those parameters. The identified modal parameters are shown in Table 2, and the fitted compliances are shown in Fig. 9. Figure 10 shows the measured and fitted equivalent dynamic compliances, and the dotted gray lines and solid black lines in Figs. 9 and 10 represent the measured and fitted compliances, respectively.

Table 2. Numerically identified modal parameters.

Modal mass		
m_{yy}	[kg]	0.0748
m_{yz}	[kg]	-0.0125
m_{zy}	[kg]	-0.0124
m_{zz}	[kg]	0.1247
Modal damping coefficient		
c_{yy}	[N/(m·s)]	7.779
c_{yz}	[N/(m·s)]	35.19
c_{zy}	[N/(m·s)]	-12.60
c_{zz}	[N/(m·s)]	45.97
Modal stiffness		
k_{yy}	[N/m]	3.912×10^{6}
k_{yz}	[N/m]	-4.678×10^{1}
k_{zy}	[N/m]	-6.700×10^{5}
k_{zz}	[N/m]	1.063×10^{7}

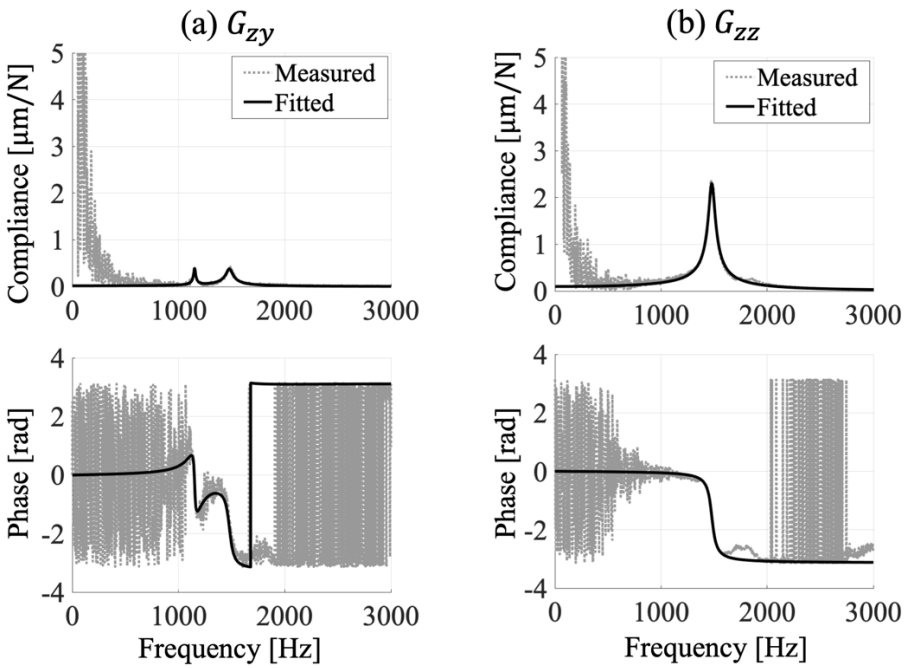

Fig. 9. Measured and fitted dynamic compliances: (a) cross dynamic compliance and (b) direct dynamic compliance.

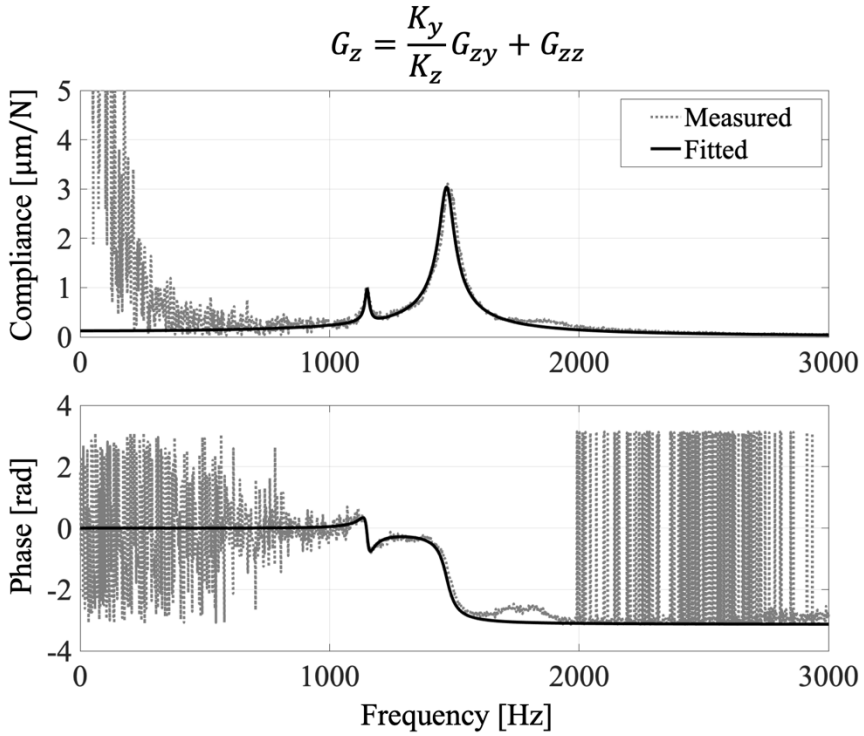

Fig. 10. Measured and fitted equivalent dynamic compliances.

4.3 Cutting experiments with CSS

Cutting experiments with CSS are conducted to confirm that the analytical stability limits agree well with the experimental results. The stability limits in CSS are also compared with those in SSV for

investigating the degree of the stability improvement by utilizing SSV.

The spindle speed signal is obtained directly from the spindle motor encoder. An accelerometer is used to measure the tool vibration during cutting. The frequency components of vibration displacement are obtained by short-time Fourier transform, and the maximum component a_{max} in each result is investigated. The cutting conditions of CSS are shown in Table 3. Note that the measurement of the specific cutting forces in the principal (y) and thrust (z) directions are carried out in advance. Since SSV will be adopted in a wide range of the spindle speed, the specific cutting force in each direction is determined in multiple spindle speeds. At each spindle speed, the feed rate, i.e., static depth of cut, is varied, and the inclination of cutting force versus feed rate is identified as the specific cutting force, i.e., the edge force is excluded. The specific cutting forces in the principal and thrust directions at all spindle speeds are averaged, and the averaged values, 1284 MPa and 711 MPa respectively as shown in Table 3, are utilized in the stability limit analysis. Note that the variations of specific cutting forces are as small as 2.5 % and 1.0 % in the principal and thrust directions, respectively, in a speed range from 1000 min^{-1} to 3000 min^{-1}.

The feed rate or static depth of cut is fixed to 0.05 mm. The cutting width, i.e., the thickness of the pipe, is changed by means of pre-cutting, and the spindle speed is set variable.

Table 3. Experimental conditions for cutting with CSS.

Workpiece properties		
Material		Brass CuZn35
Diameter D	[mm]	70
Specific cutting force in principal direction K_y	[MPa]	1284
Specific cutting force in thrust direction K_z	[MPa]	711
Tool properties		
Width (feed dir.) × Height (cutting dir.)	[mm]	25×15
Projection length	[mm]	90
Cutting condition		
Feed rate (static depth of cut) h_0	[mm/rev]	0.05
Cutting width a	[mm]	0.4, 0.6, 0.8
Spindle speed n	[min^{-1}]	1000 - 3000

The stability limit analysis in CSS is conducted with the measured equivalent dynamic compliance, and the stability limits are calculated by solving Eq. (4) [17]. The analytical and experimental results are shown in Fig. 11. Here, the dotted lines represent the results from the stability limit analysis, ○ represents the cutting result without chatter ($a_{max} < 1.5\ \mu\text{m}_{0-\text{p}}$), and × represents the cutting result with chatter ($1.5\ \mu\text{m}_{0-\text{p}} \leq a_{max}$). As can be observed in Fig. 11, the predicted stability limit and chatter frequency in each spindle speed agree well with the experimental results; e.g., in the case of a cutting width of 0.6 mm or more, chatter occurs under all spindle speed conditions. Therefore, it is confirmed that the measured equivalent dynamic compliance and specific cutting forces utilized in the stability limit analysis are valid.

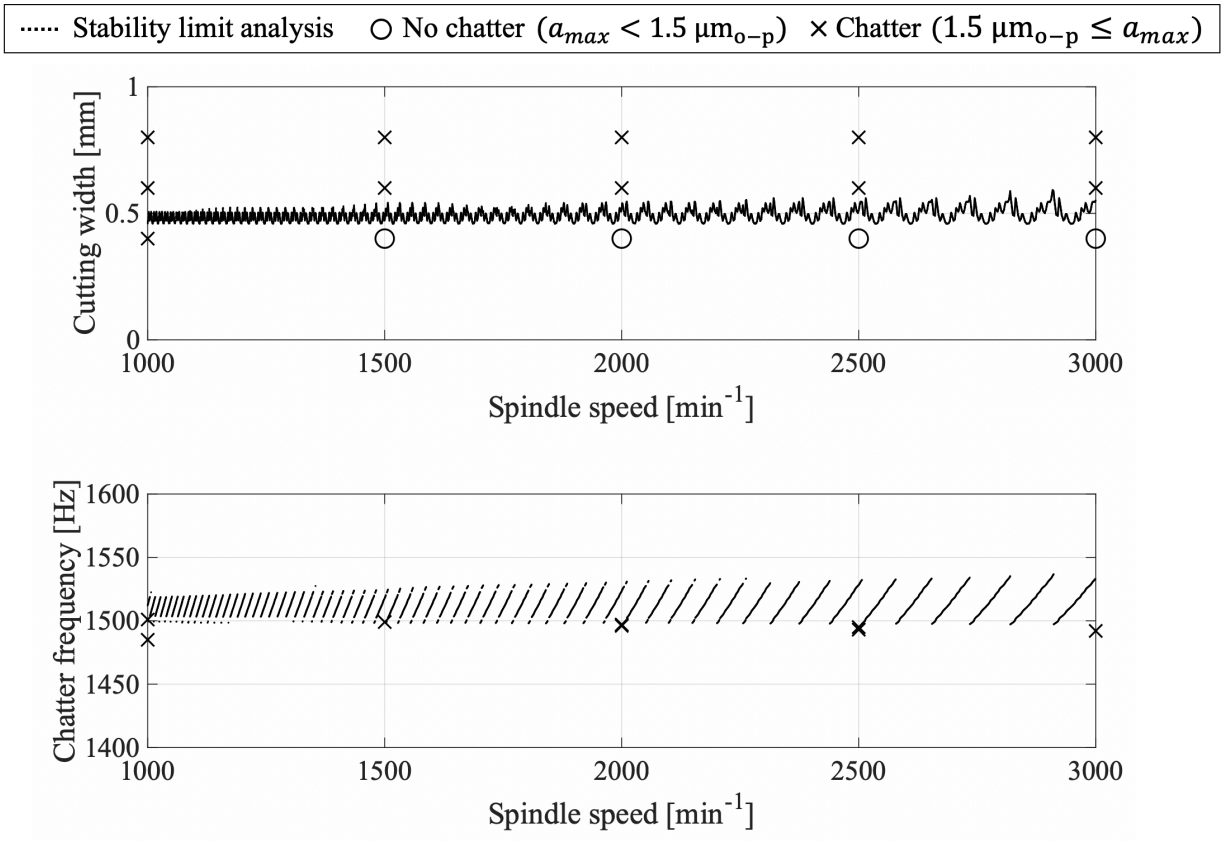

Fig. 11. Predicted stability limit and experimental results of CSS.

4.4 Cutting experiments with TSSV and comparison with time-domain simulations

Cutting experiments with TSSV are carried out by utilizing a commercially available function (Okuma Corp., Machining Navi L-*g*). Experimental conditions are shown in Table 4. Note that the values of the SSV parameters specified in Table 4 represent the set values, and the actual values are directly measured from the spindle speed signal. The value of r_a expressed in Eq. (9) is calculated by finding the moment of one revolution before from the integrated rotation angle and then calculating the proportion of the previous spindle speed to the present spindle speed. The value of the stability indices, i.e., $\overline{|r_a|}$ and N, are also calculated from the actual spindle speed. The cutting width is varied from 2.0 mm to 3.0 mm, which is about from 4 to 6 times the stability limit in CSS. The results of the cutting experiments are compared with the results of the time-domain simulations. In the simulation, the actual spindle speed signal and modal parameters shown in Table 2 are utilized. Workpiece properties and cutting conditions in the simulation are the same with the experimental ones as shown in Tables 3 and 4.

Table 4. Experimental conditions for cutting with TSSV.

SSV parameters		
Nominal spindle speed n_0	[min^{-1}]	1000, 1500, 2000
Variation period T	[sec]	0.5 - 3.5
Variation amplitude ratio RVA		0.1 - 0.5
Cutting conditions		
Feed rate (static depth of cut) h_0	[mm/rev]	0.05
Cutting width a	[mm]	2.0 - 3.0

The results of the cutting experiments and the time-domain simulations are shown in Fig. 12. Figures 12(a)-12(d) show the results in different cutting widths: (a) 2.0 mm, (b) 2.25 mm, (c) 2.5 mm, and (d) 3.0 mm. The horizontal and vertical axes represent $\overline{|r_a|}$ and N, respectively. Here, ○ represents the cutting result without chatter ($a_{max} < 1.5\ \mu m_{0-p}$), △ represents the cutting result with chatter ($1.5\ \mu m_{0-p} \leq a_{max} < 6\ \mu m_{0-p}$), and × represents the cutting result with severe chatter ($6\ \mu m_{0-p} \leq a_{max}$). In the simulation, the growing vibration in each period of SSV is considered as chatter. □ represents the simulation result without chatter, and + represents the simulation result with chatter. The results of the experiments and the simulations show good correlation. From Fig. 12, the following characteristics concerned with the experiments are found.

First, when N is almost equal, the larger the $\overline{|r_a|}$, the larger the stability. Furthermore, when $\overline{|r_a|}$ is higher than about 8 %, the chatter can be suppressed even when the cutting width is set to 3.0 mm, i.e., about 6 times higher than the stability limit of CSS. Thus, it can be said that the stability increases with an increase of $\overline{|r_a|}$ regardless of the combination of SSV parameters shown in Table 4. Therefore, $\overline{|r_a|}$ is an effective index for evaluating the stability of SSV, and hence the SSV parameters are desirable to be set so as to obtain a larger $\overline{|r_a|}$ for realizing a higher suppression effect of the chatter vibration throughout the cutting.

Second, when $\overline{|r_a|}$ is almost equal, the stability does not always increase as N increases in the experiment, e.g., A and B in Fig. 12(c). In addition, when $\overline{|r_a|}$ is smaller than 2 %, the chatter cannot be suppressed regardless of the value of N even at the smallest cutting width of 2.0 mm as shown in Fig. 12(a). From this, it can be considered that the influence of $\overline{|r_a|}$ on the chatter stability is more dominant than N, and these results are consistent with the simulation results shown in Fig. 6.

Note that some results disagree between the experiments and the simulations, e.g., A in Fig. 12(c). One reason for these disagreements can be thought to occur due to the criteria of chatter occurrence in the experiments which is judged from the magnitude of the dynamic displacement. More specifically, the smaller the N, the smaller the length of the unstable section. Hence, the chatter growth is also smaller, and this should result in a relatively smaller maximum amplitude of dynamic displacement. Therefore, when the stability of the cutting experiment is judged by the same criteria of a_{max} regardless of N, the results with a small N are likely to be more stable than the results with a large N.

Figure 13 shows an example of the experimental signals when chatter occurs which corresponds to C marked on Fig. 12(c). The cutting width is 2.5 mm, the nominal spindle speed n_0 is 1500 min^{-1}, the variation period T is 3.0 sec, and the variation amplitude ratio RVA is 0.5. The signal from the accelerometer is short-time Fourier transformed to confirm the chatter frequency and the displacement amplitude at each moment. During the cutting, the growth of chatter is observed in the transitions from the acceleration to the deceleration ($|r_a|$ is close to 0 %), and the chatter frequency changes in synchronization with the speed variation. More specifically, the chatter frequency decreases because of the negative acceleration rate. The chatter diminishes as $|r_a|$ increases, and the chatter does not grow in the transitions from deceleration to acceleration because $|r_a|$ is large in the low speed. In order to verify the constant spatial frequency f_{sc} during chatter, the comparisons of f_{sc} at times t_a, t_b, and t_c marked on Fig. 13 are investigated by utilizing Eq. (6). The spindle speeds at times t_a, t_b, and t_c are 2195 min^{-1}, 2071 min^{-1}, and 1972 min^{-1}, respectively, and the chatter frequencies at times t_a, t_b, and t_c are 1540 Hz, 1465 Hz, and 1400 Hz, respectively. The calculated spatial frequencies at times t_a, t_b, and t_c are 6.70, 6.76, and 6.78, respectively. From these results, it can be confirmed that the spatial frequencies at times t_a, t_b, and t_c are nearly the same. Therefore, the phenomena of the chatter frequency fluctuation in proportion to the spindle speed, i.e., the chatter grows up at a constant spatial frequency in SSV, is also validated experimentally.

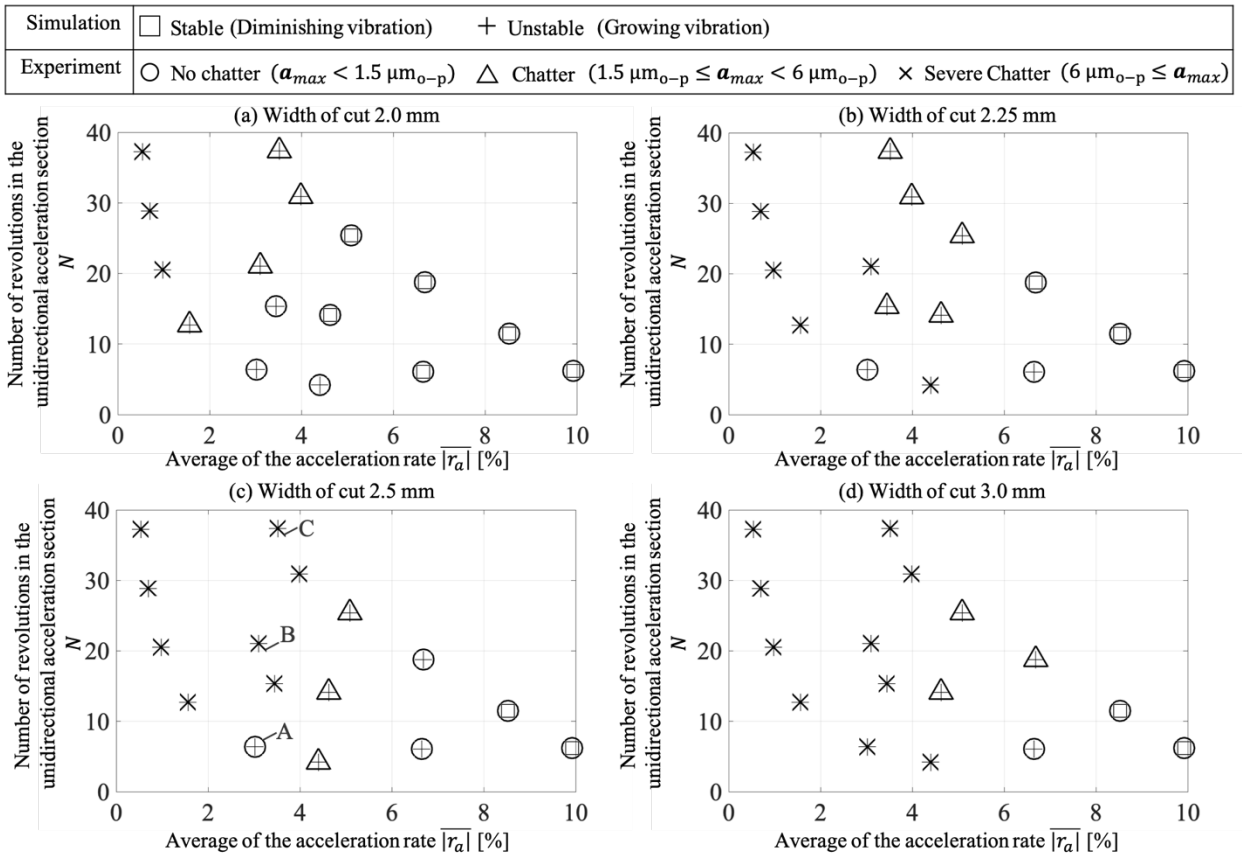

Fig. 12. Results of cutting experiments and time-domain simulations in TSSV against stability indices $\overline{|r_a|}$ and N under various cutting widths: (a) 2.0 mm, (b) 2.25 mm, (c) 2.5 mm, and (d) 3.0 mm.

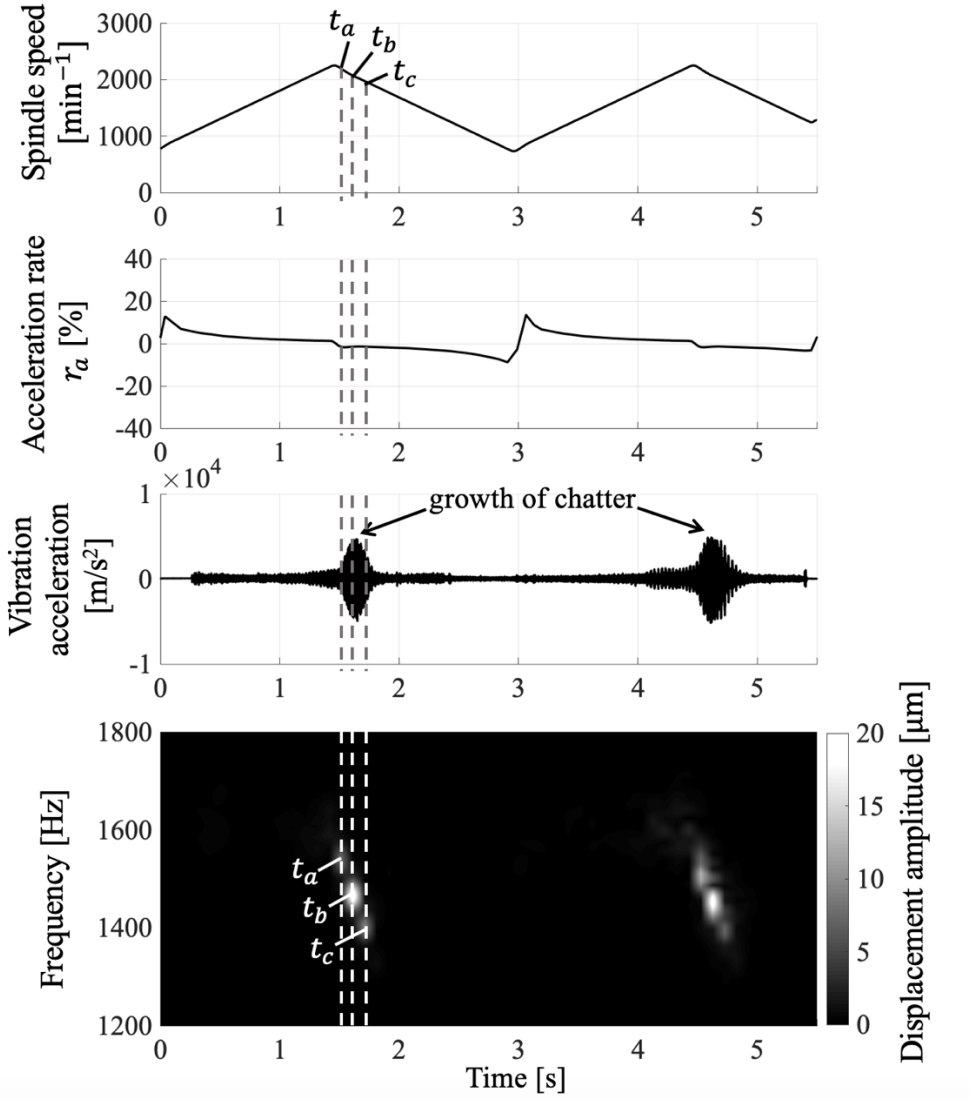

Fig. 13. Example of experimental signals of spindle speed and acceleration rate, corresponding vibration acceleration obtained from accelerometer, and short-time Fourier transform result of the vibration acceleration at unstable condition (C in Fig. 12) at a=2.5 mm, n_0=1500 min^{-1}, T=3.0 sec, and RVA=0.5 in TSSV.

5 Conclusion

The chatter growth characteristics in SSV were revealed, and the suppression effect of SSV was newly explained focusing on the fluctuation of the time chatter frequency. Even when SSV is applied, the regenerative chatter can grow with a considerably flexible structure. It was found in this study that the regenerative chatter generally grows at a constant spatial frequency in SSV (the first chatter growth characteristic). Therefore, when chatter occurs, the time chatter frequency changes at the same ratio in which the spindle speed changes, meaning that the spatial frequency is kept constant, and it brings out change of the magnitude of the dynamic compliance. Due to the change of the magnitude, the chatter can be suppressed since the dynamic compliance usually reduces as the chatter frequency changes. It was found that the chatter is likely to grow during a period where r_a is small in SSV (the second chatter growth characteristic).

Based on the reduction of the compliance, the average of the absolute acceleration rate in one period of SSV $\overline{|r_a|}$ and the number of revolutions in a unidirectional acceleration section N were proposed as novel indices to evaluate the chatter stability in SSV, i.e. larger $\overline{|r_a|}$ and N result in a larger compliance reduction.

Through the analytical investigations with the time-domain simulation, it was proved that the revealed chatter growth characteristics are valid from the following facts:

1) The time chatter frequency changes in proportion to speed variation, and the spatial frequency is kept constant.
2) The chatter growth is confirmed during the period where r_a is small.

In addition, the relations between the stability and the proposed stability indices have been investigated, and the results are summarized as follows:

1) When N is equal, the higher the $\overline{|r_a|}$, the higher the stability regardless of the variation period T and the type of SSV. This denotes that $\overline{|r_a|}$ is an effective index for evaluating the stability in SSV.

2) When $\overline{|r_a|}$ is equal, the stability is the largest at a certain N, i.e., an optimal value of N exists. This is because a larger N causes a larger dynamic compliance reduction, but on the other hand it makes sections with small $|r_a|$ longer so that chatter grows there.

3) When the values of $\overline{|r_a|}$ and N are equal, the stability limits are almost identical regardless of the combination of SSV parameters, i.e., nominal spindle speed, variation period, and variation amplitude ratio. Hence, the stability limit can be estimated by utilizing the two proposed stability indices.

4) As a comparison of SSSV and TSSV, it was confirmed that the stability limit in SSSV is always smaller than TSSV when $\overline{|r_a|}$ and N are equal. This is because $|r_a|$ near the transitions from acceleration to deceleration becomes smaller in SSSV. Furthermore, a greater stability is always achieved in TSSV than SSSV under equal variation amplitude ratio RVA even though $\overline{|r_a|}$ and N in TSSV are lower than those in SSSV.

5) When RVA and T are equal, a greater stability can be achieved under lower nominal spindle speed since $\overline{|r_a|}$ increases. This indicates that the chatter suppression effect of TSSV and SSSV decreases in high-speed region, and thus remarkable improvement of machining efficiency cannot be realized unfortunately.

A series of experiments were carried out to verify the validity of the revealed chatter growth characteristics in SSV and to confirm the effectiveness of the proposed stability indices. The results of the cutting experiments with TSSV were compared with the time-domain simulations. The experimental results showed that when N is almost equal, the larger the $\overline{|r_a|}$, the larger the stability. Furthermore, when $\overline{|r_a|}$ is higher than about 8 %, the chatter can be suppressed in all the conditions of N even when the cutting width was set to 3.0 mm, i.e., about 6 times higher than the stability limit in CSS. These results indicate that $\overline{|r_a|}$ was experimentally verified as a valid stability index as it was verified in the analytical investigations, and it is important to set appropriate SSV parameters so that $\overline{|r_a|}$ is larger than the critical value which is required for the suppression of chatter throughout the cutting. On the other hand, when the values of $\overline{|r_a|}$ are almost equal, the stability does not always increase as N increases. In addition, when $\overline{|r_a|}$ was smaller than about 2%, the chatter was not suppressed regardless of N even at the smallest cutting width. From these results, it was observed that the influence of $\overline{|r_a|}$ on the chatter stability is more dominant in comparison with N, and these results are consistent with the simulation results. The phenomena where the time chatter frequency changes at the same ratio in which the spindle speed changes, i.e., constant spatial frequency, was confirmed from the experimental signals. Finally, it was confirmed that the chatter grows during the periods where r_a is small. Hence, these denote that the revealed chatter growth characteristics are true.

References

[1] Tobias S. A., Fishwick W. Theory of regenerative machine tool chatter. The engineer 1958; 205.7: 199-203.

[2] Altintas Y, Weck M. Chatter Stability in Metal Cutting and Grinding. Annals of the CIRP 2004; 53(2):

619-642.
[3] Shamoto E., Fujimaki S., Sencer B., Suzuki N., Kato T., Hino R. A novel tool path/posture optimization concept to avoid chatter vibration in machining-Proposed concept and its verification in turning. CIRP Annals-Manufacturing Technology 2012; 61(1): 331-334.
[4] Stone B. J. The effect on the chatter behavior of machine tools of cutters with different helix angles on adjacent teeth. Proceedings of Machine Tool Design and Research Conf. 1970; 169-180.
[5] Sims N. D., Mann B., and Huyanan S. Analytical prediction of chatter stability for variable pitch and variable helix milling tools. Journal of Sound and Vibration 2008; 317(3-5): 664-686.
[6] Shamoto E., Kageyama K., Moriwaki T. Suppression of regenerative chatter vibration with irregular pitch end mill- construction of analytical model and optimization of pitch angle. Proceedings of JSME Kansai Branch Annual Meeting 2002; 024(1).
[7] Hayasaka T., Ito A., Shamoto E. Generalized design method of highly-varied-helix end mills for suppression of regenerative chatter in peripheral milling. Precision Engineering 2016; 48:45-59.
[8] Takemura T., Kitamura T., Hoshi T., Okushimo K. Active suppression of chatter by programmed variation of spindle speed. CIRP Annals 1974; 23(1): 121-122.
[9] Tsao TC., McCarthy MW., Kapor SG. A new approach to stability analysis of variable speed machining systems. International Jounal of Machine Tools and Manufacture 1993; 33(6): 791-808.
[10] Insperger T., Stepan G. Stability analysis of turning with periodic spindle speed modulation via semidiscretization. Modal Analysis 2004; 10(12): 1835-1855.
[11] Jayaram S., Kapoor S., DeVor R. Analytical stability analysis of variable speed machining. Transactions of ASME Journal of Manufacturing Science and Engineering 2000; 122:391-397.
[12] Albertelli P., et al. Spindle speed variation in turning: technological effectiveness and applicabiliity to real industrial cases. International Journal of Advanced Manufacturing Technology 2012; 62(1-4): 59-67.
[13] Al-Regib E., Ni J., Lee S. H. Programming spindle speed variation for machine tool cahtter suppression. International Journal of Machine Tools and Manufacture 2003; 43(12): 1229-1240.
[14] Otto A., Radons G. Application of spindle speed variation for chatter suppression in turning. CIRP Journal of Manufacturing Science and Technology 2013; 6(2): 102-109.
[15] Hayasaka T., Nam S., Jung H., Shamoto E., Saito K. Proposal of ‘accelerative cutting‘ for suppression of regenerative chatter. CIRP Annals 2018; 67(1): 401-404.
[16] Suzuki N, Nishimura K, Shamoto E, Yoshino K. Effect of cross transfer function on chatter stability in plunge cutting. Journal of Advanced Mechanical Design Systems and Manufacturing 2010; 4(5):883-891.
[17] Altintas Y. Manufacturing Automation. Cambridge University Press 2012; P.139-142.
[18] Seguy S., Insperger T., Arnaoud L., Dessein G., Peigne G. On the stability of high-speed milling with spindle speed variation. The International Journal of Advanced Manufacturing Technology 2010; 48(9-12): 883-895.